REGULAR ARTICLE

blood advances

Reticulocyte and red blood cell deformation triggers specific phosphorylation events

Pedro L. Moura,[1] Maria A. Lizarralde Iragorri,[2-4] Olivier Français,[5] Bruno Le Pioufle,[6] Johannes G. G. Dobbe,[7] Geert J. Streekstra,[7] Wassim El Nemer,[2-4] Ashley M. Toye,[1,8,9,*] and Timothy J. Satchwell[1,8,9,*]

[1]School of Biochemistry, University of Bristol, Bristol, United Kingdom; [2]Université de Paris, Biologie Intégrée du Globule Rouge Unité Mixte de Recherche_S1134, INSERM, Université de la Réunion, Institut National de la Transfusion Sanguine, Paris, France; [3]Institut National de la Transfusion Sanguine, Paris, France; [4]Laboratoire d'Excellence GR-Ex, Paris, France; [5]ESIEE-Paris, Unité Électronique, Systèmes de Communication et Microsystèmes FRE2028, University Paris-Est, Noisy Le Grand, France; [6]École Normale Supérieure Paris-Saclay, Le Centre National de la Recherche Scientifique Institut d'Alembert, Systèmes et Applications des Technologies de l'Information et de l'Énergie, Université Paris, Saclay, France; [7]Department of Biomedical Engineering and Physics, Amsterdam University Medical Center, University of Amsterdam, Amsterdam, The Netherlands; [8]Bristol Institute for Transfusion Sciences, National Health Service Blood and Transplant, Bristol, United Kingdom; and [9]National Institute for Health Research Blood and Transplant Research Unit in Red Cell Products, University of Bristol, Bristol, United Kingdom

Key Points

- Specific phosphorylation events are associated with RBC deformation.
- Inhibition of GSK3 and Lyn impairs RBC capacity to undergo successive deformation and resist shear stress.

The capacity to undergo substantial deformation is a defining characteristic of the red blood cell (RBC), facilitating transit through the splenic interendothelial slits and microvasculature. Establishment of this remarkable property occurs during a process of reticulocyte maturation that begins with egress through micron-wide pores in the bone marrow and is completed within the circulation. The requirement to undertake repeated cycles of deformation necessitates that both reticulocytes and erythrocytes regulate membrane-cytoskeletal protein interactions in order to maintain cellular stability. In the absence of transcriptional activity, modulation of these interactions in RBCs is likely to be achieved primarily through specific protein posttranslational modifications, which at present remain undefined. In this study, we use high-throughput methods to define the processes that underlie the response to deformation and shear stress in both reticulocytes and erythrocytes. Through combination of a bead-based microsphiltration assay with phosphoproteomics we describe posttranslational modification of RBC proteins associated with deformation. Using microsphiltration and microfluidic biochip-based assays, we explore the effect of inhibiting kinases identified using this dataset. We demonstrate roles for GSK3 and Lyn in capillary transit and maintenance of membrane stability following deformation and show that combined inhibition of these kinases significantly decreases reticulocyte capacity to undergo repeated deformation. Finally, we derive a comprehensive and integrative phosphoproteomic dataset that provides a valuable resource for further mechanistic dissection of the molecular pathways that underlie the RBC's response to mechanical stimuli and for the study of reticulocyte maturation.

Introduction

The capacity to undergo substantial deformation is a defining characteristic of the red blood cell (RBC). Establishment of this remarkable property occurs during a process of reticulocyte maturation that begins in the bone marrow and is completed within the circulation in which the nascent reticulocyte, having expelled its nucleus, remodels its membrane to acquire the recognizable biconcave morphology of the

Submitted 5 June 2019; accepted 22 July 2019. DOI 10.1182/bloodadvances.2019000545.

*A.M.T. and T.J.S. contributed equally to this work.

For original data, please contact t.satchwell@bristol.ac.uk or ash.m.toye@bristol.ac.uk.

The mass spectrometry proteomics data have been deposited to the ProteomeXchange Consortium via the PRIDE[47] partner repository with the dataset identifiers PXD013652 and PXD013960, with corresponding DOIs 10.6019/PXD013652 and 10.6019/PXD013960.

The full-text version of this article contains a data supplement.

mature erythrocyte. While the deformability of early reticulocytes is known to be lower than that of erythrocytes[1-3] but increase progressively throughout the maturation process, reticulocytes themselves must undergo extreme deformations without damage or lysis. These include bone marrow egress (before entering peripheral circulation) as well as multiple traversals of the splenic interendothelial slits (during circulatory maturation) and the microvasculature. As a result, reticulocytes are necessarily exposed to high pressures and shear stress, which in turn may partially drive the processes underlying maturation.

Modulation of reticulocyte and erythrocyte properties through response to shear stress is a well described phenomenon. Shear stress has been reported to be implicated in the regulation of adenosine triphosphate (ATP) release by erythrocytes,[4,5] removal of autophagic vesicles from circulating reticulocytes,[6] and general induction of autophagy in other mammalian cells.[7] In erythrocytes, shear stress is known to induce calcium ion entry through activation of the mechanically activated cation channel Piezo1,[8] regulating the volume changes necessary for the maintenance of homeostasis during deformation.[9] Increases in intracellular calcium are known to promote phosphorylation of multiple proteins through interaction with sensors such as calmodulins and C2 domain-containing proteins.[10-13] Phosphorylation, in turn, regulates cytoskeletal alterations and interactions[14,15] as well as the stability of the erythrocyte membrane.[10,16]

Understanding the biochemical mechanisms that enable or are activated upon RBC deformation is an extremely difficult proposition given the challenges associated with isolating cells undertaking this process. Various types of shear stress/deformation-inducing systems exist specifically for the study of RBC properties,[17-19] but most of the focus of the use of those systems has been on the assessment of the mechanical and physical properties of the cells or the high-throughput screening of chemical compound effects on these characteristics[20] rather than elucidation of the molecular basis of RBC deformation.

In this study, we aim to better define the phosphorylation events that underlie the response to deformation and shear stress in both reticulocytes and erythrocytes. Using in vitro systems that mimic deformation through the spleen and microvasculature, respectively, we have captured cells in states immediately pre-, mid-, and postdeformation and used phosphoproteomics to obtain a unique and comprehensive shear-response dataset, providing a valuable resource for further studies of the processes involved in RBC deformation and reticulocyte maturation. We then validate the importance of 2 of these modifications in the cellular response to shear stress through chemical inhibition of the respective proteins.

Methods

Erythrocyte isolation and in vitro erythroid culture

Erythrocytes were isolated by leukofiltration from the RBC fraction obtained by Histopaque separation of healthy donor platelet apheresis waste blood. In vitro–cultured reticulocytes were differentiated from $CD34^+$ cells isolated from the mononuclear cell fraction according to previously published protocols.[21] All source material was provided with written informed consent for research use given in accordance with the Declaration of Helsinki (National Health Service Blood and Transplant, Filton, Bristol, United Kingdom). The research into the mechanisms of erythropoiesis was reviewed and approved by the Bristol Research Ethics committee (REC Number 12/SW/0199).

Proteomics experimental design, data acquisition and analysis

Two experiments were performed: (1) A comparison of erythrocytes and in vitro–derived reticulocytes lysed before, during, and after shear stress exposure through microsphere filtration (microsphiltration) was performed, with at least 3 biological repeats per cell type and shear stress exposure condition, generating a total of 21 individual samples that were processed through qualitative titanium dioxide–enriched phosphoproteomics; and (2) a comparison of reticulocytes lysed before and after shear stress exposure through passage in successive microfluidic constrictions with 3 biological repeats and generating a total of 6 individual samples.

Each sample corresponds to 10×10^6 cells. The protein content between samples was equalized through hemoglobin estimation via the use of Drabkin's reagent, using different standard curves for reticulocytes and erythrocytes due to their differences in average hemoglobin concentration. Data are available via ProteomeXchange with identifiers PXD013652 and PXD013960, with corresponding DOIs 10.6019/PXD013652 and 10.6019/PXD013960. Further information and reasoning for the chosen proteomics design may be found in the supplemental Rationale material. Extended methods for sample preparation, data acquisition and analysis are provided in the supplemental Methods.

ARCA sample preparation and analysis

A total of 2×10^6 cells were diluted in 200 μL of a polyvinylpyrrolidone solution (viscosity, 28.1 mPa·s; Mechatronics Instruments). Samples were assessed in an Automated Rheoscope and Cell Analyzer (ARCA)[22] according to previously published protocols.[23] At least 1500 valid cells per sample were analyzed using bespoke ARCA analysis software.

Microsphiltration

A microsphiltration device was built as originally described by Deplaine et al.[24] A 1:1 mixture of 15 to 25 μm and 5 to 15 μm diameter metal microspheres (1 g; 1 g consisting of 96.50% tin, 3.00% silver, and 0.50% copper; Industrie des Poudres Sphériques) was resuspended in 5 mL PBSAG (phosphate-buffered saline + 1 mg/mL bovine serum albumin + 2 mg/mL glucose). A total of 600 μL of the microsphere suspension were loaded directly on top of the antiaerosol filter of the inverted pipette tip. The remaining volume was filled with PBSAG. A 50-mL syringe was loaded with PBSAG and connected to a 3-way stopcock, which was connected to the pipette tip using silicone tubing (Cole-Parmer). A 1-mL syringe was used for loading the cell suspension into the microsphiltration system through the stopcock. Pressure was created manually through slow and constant depression of the 50-mL syringe plunger.

For the proteomics experiment, cells were lysed at 3 points: (1) before use of the microsphiltration system, (2) during the point of maximum cell density in the bead layer, and (3) postrecovery of the cells from the microsphiltration system. For recovery during the point of maximum cell density in the bead layer, pressure was stopped immediately, and the top of the pipette filter tip was cut open. Then, the PBSAG present in the system was aspirated. Forty microliters of lysis buffer were carefully added to the bead layer and incubated for 10 minutes at 4°C. The bead layer and lysate were collected into a microcentrifuge tube and centrifuged for 10 minutes

at 16 100*g*, 4°C. The supernatant was then collected. For recovery after the microsphiltration system, the resulting suspension was centrifuged for 5 minutes at 400*g*, 4°C, and the cells were counted and lysed. Lysates were then equalized in regard to cell number through quantitation of hemoglobin using Drabkin's reagent.

For the percentage of cell recovery experiment, cells were treated overnight with 1:1000 dimethyl sulfoxide (DMSO) as a control, or a pharmacological inhibitor (3 μM bafetinib [specific Lyn inhibitor, 50% inhibition concentration (IC_{50}): 19 nM; Insight Biotechnology], 10 nM CHIR-98014 [specific GSK3 inhibitor, GSK3α IC_{50}: 0.65 nM, GSK3β IC_{50}: 0.58 nM, closest homolog Cdc2 IC_{50}: 3.7 μM; Stratech Scientific], or a combination of both). Following treatment, the cells were stained with CellTracker Green CMFDA Dye (Invitrogen) for 45 minutes at 37°C. After staining, the cells were mixed with untreated, unstained cells in a 5:95 mixture and resuspended in PBSAG. The resulting cell suspension was subjected to microsphiltration and analyzed through flow cytometry.

For fixation of cells in the bead layer, the filter tip was cut and the PBSAG aspirated as described earlier. A total of 100 μL of fixing solution (1% paraformaldehyde and 0.0075% glutaraldehyde [v/v] in PBSAG) were carefully added to the bead layer and incubated for 10 minutes at room temperature. One milliliter of PBSAG was added for resuspension of the bead layer and the suspension was collected into microcentrifuge tubes. The beads were let to sediment by gravity and, 5 minutes later, the supernatant containing the fixed cells was collected into new microcentrifuge tubes. The cell suspension was centrifuged, and the cells were washed twice in PBSAG to remove any remaining microbeads. The fixed cells were then stored at 4°C.

Microfluidic multiconstriction assay

The microfluidic biochip was designed and fabricated as described by Lizarralde Iragorri et al.[19] An MFCS-EZ microfluidic flow control system (Fluigent) was used to regulate the flow pressure in the microfluidic biochip. The biochip was connected to the pump by 1.6-mm silicone tubing and male Luer connectors and mounted on the stage of an inverted AxioObserver Z1 microscope (Zeiss) coupled with a Phantom Miro M 320S high-speed camera, with imaging at ×100 magnification.

For each assay, 60 μL of reticulocyte or erythrocyte suspensions at 2.5% hematocrit were loaded in the input well of the biochip and perfused at constant pressure (150 mBar). The 2.5% hematocrit, lower than the literature value of 30%, was used to allow for the identification of individual cells in the acquired images. For inhibitor treatment, the cells were treated with 1:1000 DMSO as a control, or an adequate inhibitor (3 μM bafetinib, 10 nM CHIR-98014, or a combination of both) for an hour and resuspended in PBS with the respective inhibitor for use in the microfluidics chip. High-speed videos were obtained at 900 to 1500 frames per second and converted into .tiff frame sequences with the use of Phantom Camera Control (PCC) v2.2 or Cine Viewer (CV) v3.1 software.

High-speed video analysis

All images resulting from the high-speed videos were processed with the use of Fiji v. 2.0.0-rc-54/1.51h.[25] A detailed method for high-speed video analysis is provided in the supplemental Methods.

Raw proteomics data and data preprocessed with Proteome Discoverer are available via ProteomeXchange with identifiers PXD013652 and PXD013960, with corresponding DOIs 10.6019/PXD013652 and 10.6019/PXD013960. Proteomics data tables from preprocessing with Proteome Discoverer may also be found in the supplemental Data.

Filtered proteomics data from the microsphiltration and microfluidics proteomics analyses may be respectively found in supplemental Tables 1 and 2.

Results

The RBC phosphoproteome is modulated in response to deformation

Due to the relatively short timeframe required for the deformation and recovery of RBCs and the general lack of transcriptional machinery, we hypothesized that any underlying mechanism for responding to deformation would necessarily be driven by post-translational modification of proteins via phosphorylation. Altered phosphorylation of cytoskeletal and membrane proteins is known to influence multiple properties in the erythrocyte (eg, membrane stability and tension, deformability, effective viscosity[16,26-28]), principally through changes in cytoskeletal stability and in the association between cytoskeletal proteins and the multiprotein membrane complexes. Given the reported increased kinase activity of reticulocytes[29] and the fact that many proteins are lost during reticulocyte maturation to the erythrocyte,[30] investigating reticulocyte response to deformation may allow for increased sensitivity in the detection of deformation-induced signaling cascades. Thus, to investigate any possible changes underlying deformation and recovery, we produced 2 qualitative phosphoproteomics datasets comparing erythrocytes from 3 donors and in vitro $CD34^+$-derived cultured reticulocytes from 4 donors lysed before, during, and after passage through the spleen-like microsphiltration system originally developed by Deplaine et al.[24] In vitro–generated reticulocytes were used in preference to reticulocytes isolated from donors because of the high number of cells required per complete sample set in the microsphiltration experiment, although we have previously shown that in vitro and in vivo reticulocytes are proteomically similar both in quantitative protein abundance and presence of specific phosphopeptides.[23]

Figure 1A summarizes the design of the experiment and includes micrographs of erythrocytes in the 3 conditions. Cells analyzed in the beginning of the experiment possess the characteristic biconcave morphology, whereas a majority of the cells fixed during passage through the microsphiltration system are in the process of being deformed (although the degree to which they are deformed varies for each cell). Cells that have undergone passage through the system regain their biconcave morphology without any visible alteration. Resulting processed proteomics data from the experiment may be found in supplemental Table 1.

A significant proportion of the detected phosphopeptides were unique to the deformed or recovery states in erythrocytes (52.4% of detected phosphopeptides) and reticulocytes (24.3% of detected phosphopeptides), as summarized in Figure 1B. Further analysis of these phosphopeptide groups through use of the STRING database revealed a predicted common underlying protein-protein interaction network, which is shown in Figure 1C. Two main groups of proteins were observed to be connected through this network, namely kinases and intracellular transport proteins (as identified by

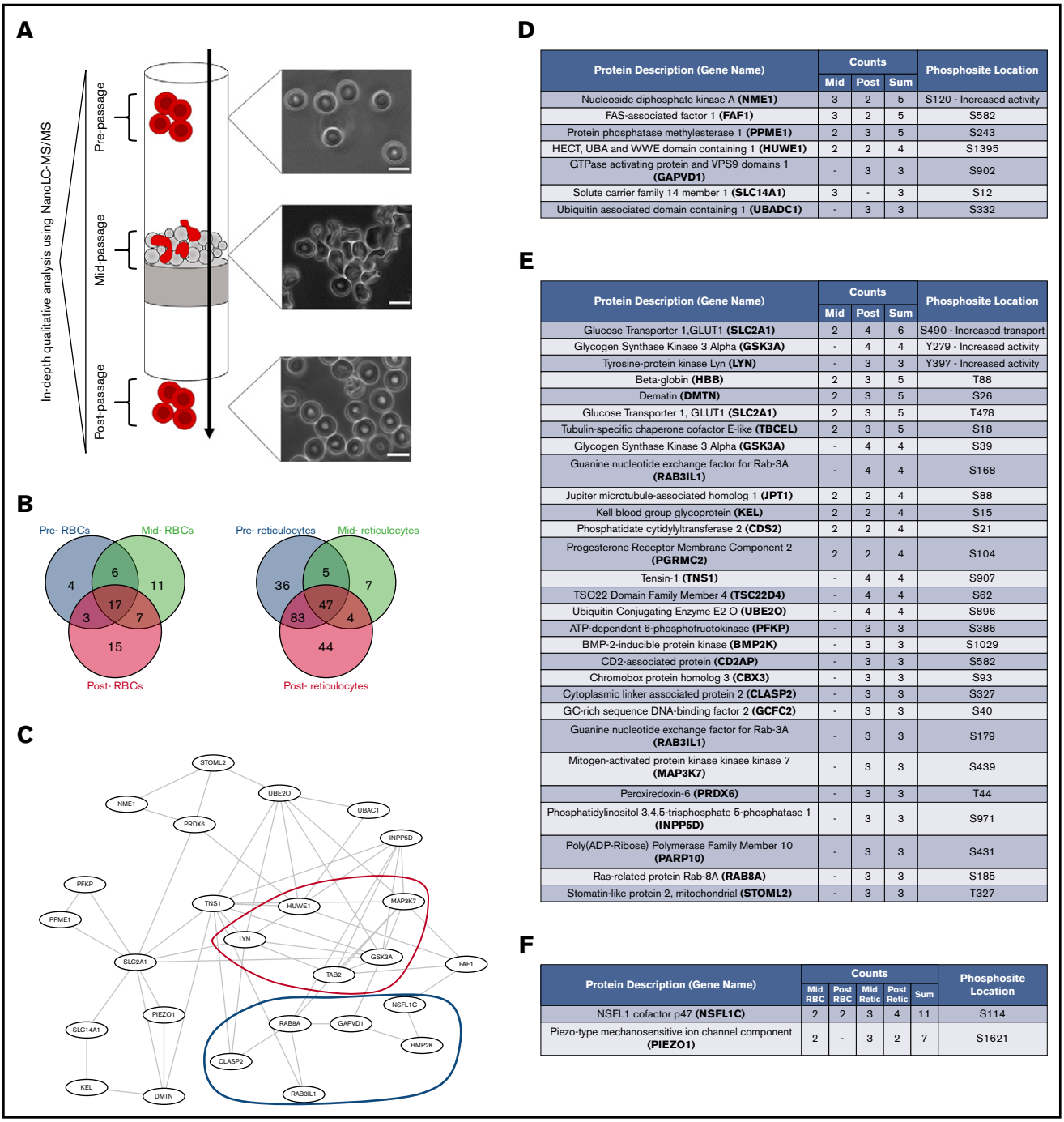

D

Protein Description (Gene Name)	Counts			Phosphosite Location
	Mid	Post	Sum	
Nucleoside diphosphate kinase A **(NME1)**	3	2	5	S120 - Increased activity
FAS-associated factor 1 **(FAF1)**	3	2	5	S582
Protein phosphatase methylesterase 1 **(PPME1)**	2	3	5	S243
HECT, UBA and WWE domain containing 1 **(HUWE1)**	2	2	4	S1395
GTPase activating protein and VPS9 domains 1 **(GAPVD1)**	-	3	3	S902
Solute carrier family 14 member 1 **(SLC14A1)**	3	-	3	S12
Ubiquitin associated domain containing 1 **(UBADC1)**	-	3	3	S332

E

Protein Description (Gene Name)	Counts			Phosphosite Location
	Mid	Post	Sum	
Glucose Transporter 1,GLUT1 **(SLC2A1)**	2	4	6	S490 - Increased transport
Glycogen Synthase Kinase 3 Alpha **(GSK3A)**	-	4	4	Y279 - Increased activity
Tyrosine-protein kinase Lyn **(LYN)**	-	3	3	Y397 - Increased activity
Beta-globin **(HBB)**	2	3	5	T88
Dematin **(DMTN)**	2	3	5	S26
Glucose Transporter 1, GLUT1 **(SLC2A1)**	2	3	5	T478
Tubulin-specific chaperone cofactor E-like **(TBCEL)**	2	3	5	S18
Glycogen Synthase Kinase 3 Alpha **(GSK3A)**	-	4	4	S39
Guanine nucleotide exchange factor for Rab-3A **(RAB3IL1)**	-	4	4	S168
Jupiter microtubule-associated homolog 1 **(JPT1)**	2	2	4	S88
Kell blood group glycoprotein **(KEL)**	2	2	4	S15
Phosphatidate cytidylyltransferase 2 **(CDS2)**	2	2	4	S21
Progesterone Receptor Membrane Component 2 **(PGRMC2)**	2	2	4	S104
Tensin-1 **(TNS1)**	-	4	4	S907
TSC22 Domain Family Member 4 **(TSC22D4)**	-	4	4	S62
Ubiquitin Conjugating Enzyme E2 O **(UBE2O)**	-	4	4	S896
ATP-dependent 6-phosphofructokinase **(PFKP)**	-	3	3	S386
BMP-2-inducible protein kinase **(BMP2K)**	-	3	3	S1029
CD2-associated protein **(CD2AP)**	-	3	3	S582
Chromobox protein homolog 3 **(CBX3)**	-	3	3	S93
Cytoplasmic linker associated protein 2 **(CLASP2)**	-	3	3	S327
GC-rich sequence DNA-binding factor 2 **(GCFC2)**	-	3	3	S40
Guanine nucleotide exchange factor for Rab-3A **(RAB3IL1)**	-	3	3	S179
Mitogen-activated protein kinase kinase kinase 7 **(MAP3K7)**	-	3	3	S439
Peroxiredoxin-6 **(PRDX6)**	-	3	3	T44
Phosphatidylinositol 3,4,5-trisphosphate 5-phosphatase 1 **(INPP5D)**	-	3	3	S971
Poly(ADP-Ribose) Polymerase Family Member 10 **(PARP10)**	-	3	3	S431
Ras-related protein Rab-8A **(RAB8A)**	-	3	3	S185
Stomatin-like protein 2, mitochondrial **(STOML2)**	-	3	3	T327

F

Protein Description (Gene Name)	Counts					Phosphosite Location
	Mid RBC	Post RBC	Mid Retic	Post Retic	Sum	
NSFL1 cofactor p47 **(NSFL1C)**	2	2	3	4	11	S114
Piezo-type mechanosensitive ion channel component **(PIEZO1)**	2	-	3	2	7	S1621

Figure 1. Red blood cell deformation induces measurable changes in the phosphoproteome. (A) Experimental design for proteomic comparison: RBCs and cultured reticulocytes were subjected to flow in a microsphiltration system and lysed before, during, and after passage. The lysates were equalized through hemoglobin quantification using Drabkin's reagent and analyzed through NanoLC-MS/MS. Cells were fixed and imaged under brightfield at all 3 stages, showing the extent of their deformation within the system and their recovery after passage. Scale bars, 10 μm. (Microsphiltration schematic adapted from Duez et al.[48]) (B) Venn diagram of differentially phosphorylated proteins with ≥50% detection across all samples in RBCs (left, n = 63 with 33 modifications detected exclusively in cells mid- and postdeformation) and reticulocytes (right, n = 226 with 55 modifications detected exclusively in cells mid- and postdeformation). (C) Top-scoring protein-protein interaction network from the joint dataset of mid- and postdeformation exclusive phosphoproteins in reticulocytes, as predicted by STRING.[49] Two main subsets of proteins were present in the network, kinases (marked in red) and vesicle transport-related proteins (marked in dark blue). (D) List of phosphoproteins exclusive to the RBC mid-deformation and mid-/postintersection datasets. Count indicates the number of observed instances of the phosphopeptide (n = 3); the phosphopeptides were sorted by the sum of their counts in both datasets and filtered for their presence in at least 2 samples per condition. PhosphoSite location indicates the predicted location of the phosphorylation site in the protein sequence (as predicted by SEQUEST and/or PhosphoSitePlus data[50]), as well as the effect of its phosphorylation if described in low-throughput studies according to PhosphoSitePlus.[50] (E) List of phosphoproteins exclusive to the reticulocyte mid-deformation and mid-/postintersection datasets (n = 4). Dataset analysis, filtering, and annotation were performed as previously described. (F) List of phosphoproteins present among both reticulocyte and RBC mid-/postdeformation datasets, with no significant detection in the predeformation dataset; dataset analysis, filtering, and annotation were performed as previously described.

red and blue outlines, respectively). The only KEGG pathway detected in the dataset through enrichment analysis was related to AMPK signaling (KEGG enrichment performed with the use of DAVID 6.8,[31,32] $P = .029$), although no AMPK-related phosphopeptides were detected (suggesting we are capturing downstream phosphorylation events). Phosphopeptides detected only in erythrocytes are listed in the table in Figure 1D, whereas phosphopeptides detected only in reticulocytes are listed in Figure 1E. As expected, a much broader variety of novel peptides phosphorylated during or after deformation was detected in reticulocytes compared with erythrocytes. Although this finding may be related to the previously mentioned higher kinase activity in reticulocytes,[29] it may also potentially highlight the existence of only a temporary role for the detected proteins and respective phosphorylations. Interestingly, only a small overlap was detected between erythrocytes and reticulocytes (Figure 1F), which could also be related to differences in the activation kinetics for signaling and recovery of the cell from deformation (or, again, due to known differences in kinase abundances between the cell types). It is noteworthy that only the phosphopeptide corresponding to NSFL1C was consistently detected among the 2 cell types in both the mid- and postdeformation states, despite no information existing on its effect in erythroid cells.

Inhibition of Lyn and GSK3 decreases RBC capacity to undergo repeated deformation

Notably, phosphorylations with well-defined effects on kinase activity were also detected by our experimental approach in reticulocytes. Because of the ubiquitous presence of their phosphopeptides in the reticulocyte postdeformation samples, we focused our attention on the kinases Lyn and GSK3α. The tyrosine kinase Lyn is a known regulator of the erythrocyte protein band 3, a cytoskeleton-interacting protein known to be the most abundant membrane protein in RBCs.[33] Its kinase activity is partially regulated through autophosphorylation of the tyrosine residue in site Y397, which was detected in this dataset and has been well-described to induce further activation of the protein.[34] Conversely, serine/threonine kinases of the GSK3 family have been shown to participate in the phosphorylation of β-adducin,[35] which is also known to interact with the spectrin-actin cytoskeleton in erythrocytes.[36] Tyrosine phosphorylation of GSK3α at the Y279 site, which we have detected in this dataset, is known to increase enzymatic activity.[37]

Given that modulating the activity of both kinases could have a quantifiable impact on the erythroid cytoskeleton, we decided to attempt chemical inhibition and subsequent cell microsphiltration to investigate a putative effect on the ability of reticulocytes to undergo successive deformations. In addition to the 2 kinase inhibitors, treatment with an anti-glycophorin A (GPA) antibody was used as a positive control for detrimental effects on cell deformability, as GPA ligation has been demonstrated to increase cell rigidity.[38] After treatment, the cells were mixed at approximately 5:95 ratio with untreated erythrocytes, as per a previously published method by Cluitmans et al,[39] and allowed to settle on the surface of the microbead layer. Even, manual pressure was applied and the percentage of reticulocytes that traversed the system was evaluated using flow cytometry through the detection of CellTracker Green CMFDA-labeled cells. The results for this experiment are shown in Figure 2A.

Predictably, pretreatment with the anti-GPA antibody significantly affected cell traversal through microsphiltration. Inhibition of Lyn kinase showed a nonsignificant reduction in the percentage of cells obtained after passage through the system, whereas inhibition of GSK3 showed a significant reduction that was comparable to treatment with the anti-GPA antibody. Importantly, and in contrast to cells treated with the anti-GPA antibody, treatment with either inhibitor did not affect intrinsic capacity to undergo initial deformation as assayed through the Deformability Index distributions obtained by an Automated Rheoscope and Cell Analyzer (supplemental Figure 1). To further investigate the effect of inhibiting these 2 kinases, we used a microfluidics-based system (previously published by Lizarralde-Iragorri et al[19]) to subject the cells to shear stress and successive deformations in an observable manner. The chip is shown in Figure 2B, with an accompanying example of cells passing through the system (which may also be observed in supplemental Video 1) and being subjected to automatic tracking (supplemental Video 2). Through use of this system, we identified a general decrease in microcapillary traversal velocity in both reticulocytes and erythrocytes after treatment to inhibit Lyn or GSK3, as summarized in Figure 2C. In cases in which the comparison P value was higher than the significance cutoff, a decrease in cell velocity is still observed across all samples, with a large variation between samples causing the low significance.

Concomitant treatment with both inhibitors had a compounding effect, resulting in near-complete inability of cells to traverse the microfluidics chip and leading to highly variable results (eg, complete blockage of the system led to extremely slow traversal as shown in supplemental Video 3). We thus identify for the first time a requirement for both Lyn and GSK3 for regulating the capacity of cells to undergo successive deformations and resist shear stress.

Cells passing through the microfluidics system can be lysed near-immediately after deformation (we estimate there to be a maximum interval of 3 seconds between the last constriction point and the end of the capillary traversal), an interval that we considered significantly different to the approximately 5-minute period necessary to obtain samples following microsphiltration. Therefore, we combined the phosphoproteomics data from both experiments to create a comprehensive integrative dataset (shown in Table 1, with processed phosphoproteomics data from the microfluidics experiment provided in supplemental Table 2), which lists the phosphorylation sites most likely to be modulated as a result of shear stress recognition in the reticulocyte, generating a unique and unprecedented dataset that characterizes a highly transient state of this dynamic cell.

Discussion

Studying the dynamic processes involved in reticulocyte maturation or changes in the erythrocyte in response to mechanical stimulus presents inherent challenges due to the short-lived nature of said processes and, consequently, the technical difficulties of obtaining cells in a physiologically relevant state of deformation/posttranslational modification. Previous proteomic studies of the RBC and reticulocyte have mostly focused mainly on deriving definitive descriptive proteomes or studying quantitative differences in protein content between these cell types,[23,40-43] although we have also recently published a dataset that characterizes important differential phosphorylation between erythrocytes and endogenous/cultured reticulocytes.[23]

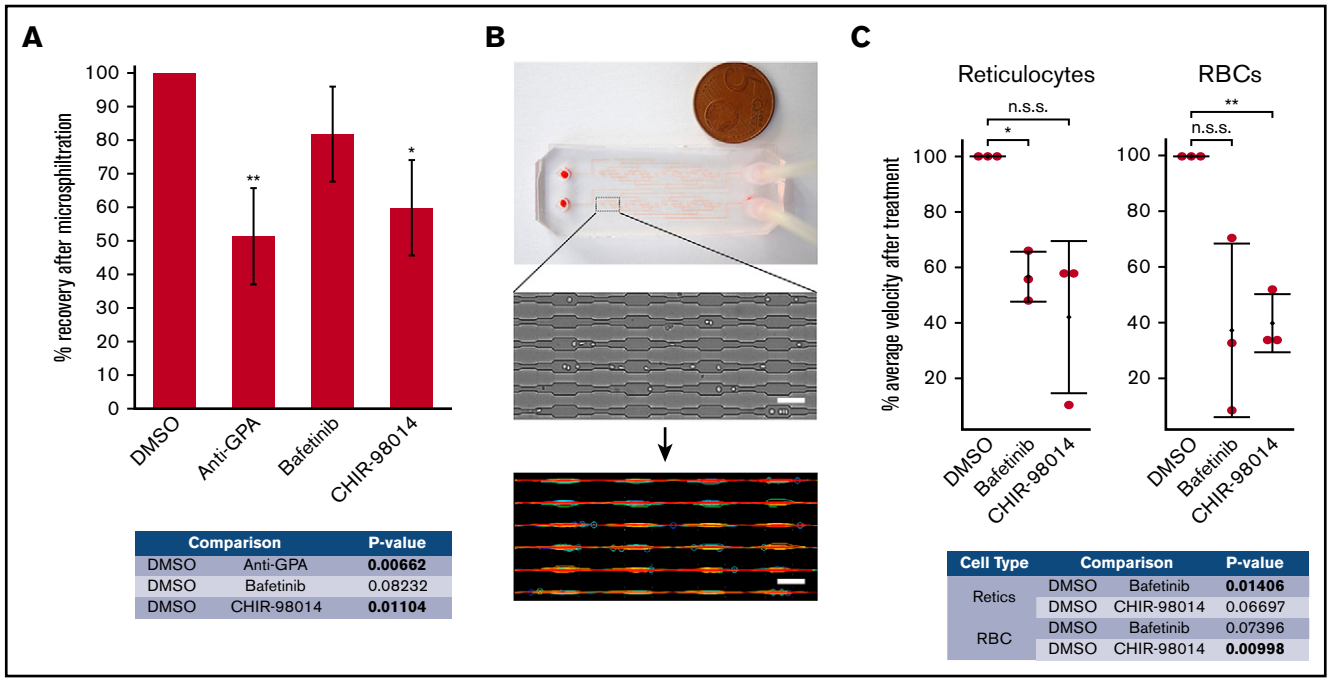

Comparison		P-value
DMSO	Anti-GPA	**0.00662**
DMSO	Bafetinib	0.08232
DMSO	CHIR-98014	**0.01104**

Cell Type	Comparison		P-value
Retics	DMSO	Bafetinib	**0.01406**
	DMSO	CHIR-98014	0.06697
RBC	DMSO	Bafetinib	0.07396
	DMSO	CHIR-98014	**0.00998**

Figure 2. GSK3 and Lyn inhibition impacts capillary traversal of reticulocytes and red blood cells. (A) Percentage recovery of reticulocytes treated with the respective reagent after microsphiltration. After treatment, the cells were added to an untreated RBC suspension in a 5:95 ratio and the mixture then subjected to microsphiltration. Anti-GPA antibody was used as a positive control for negative effects on cell deformability. Bafetinib (3 μM) was used as a Lyn inhibitor and CHIR-98014 (10 nM) was used as a GSK3 inhibitor. Error bars correspond to the standard deviation (n = 3). All comparisons were performed with a paired 2-tailed Student *t* test. The *P* values for each comparison are shown below the bar graph. $*P < .05$, $**P < 0.01$. (B) Image of the microfluidic PDMS biochip used for the capillary traversal experiment. The magnified image shows a section of the microcapillary channels, through which reticulocytes and red blood cells were subjected to successive deformations. Frame sequences were obtained through the use of a high-speed camera and then subjected to image analysis for automated cell tracking with the use of TrackMate.[51] Scale bars, 50 μm. (C) Percentage microcapillary traversal velocity of reticulocytes and red blood cells treated with the respective reagents. The cells were treated for a minimum period of 1 hour and subjected to passage through the microfluidic biochip. The graph shows the average cell microcapillary traversal velocity of each treated sample as a percentage of the respective DMSO control sample traversal velocity. All comparisons were performed with a 1-sample Student *t* test. The error bars correspond to the standard deviation (n = 3). The *P* values for each comparison are shown below the dot plot. $*P < .05$, $**P < .01$. A minimum of 1000 cell tracks were analyzed per sample. n.s.s., not statistically significant.

However, none of these studies have investigated the possibility of posttranslational modifications actively changing within the cell over time as a direct consequence of the physiological stress involved in circulation. Previous studies have indicated that signaling pathways are at least involved in the changes induced in RBC aging,[13] but the use of pharmacological compounds to induce a response will most likely generate outcomes that range beyond what the cell normally experiences.

Therefore, in this study, we report the first qualitative phosphoproteomic dataset that dissects the response to deformation and shear stress in the human reticulocyte and erythrocyte, identifying previously unreported protein modifications and signaling pathways and investigating the impact of inhibiting part of those pathways.

To achieve this, we have combined the use of 2 established systems that mimic physiological deformation of RBCs[19,24] with high-throughput proteomics based on titanium dioxide enrichment, allowing us to investigate the difference in phosphorylation events present before, during and after deformation. By combining datasets derived from systems that mimic splenic passage and capillary deformation, we identify posttranslational modifications in several reticulocyte membrane and cytoskeletal proteins, including ankyrin, dematin, α/β-spectrin, and Piezo1, which we show are associated with mechanical stimulus and hypothesize may be modulated as part of the shear-induced reticulocyte maturation process due to their detection in reticulocytes occurring only after exposure to deformation.

Focusing on the signaling pathways that seemingly activate upon reticulocyte deformation, we used pharmacological kinase inhibitors to inhibit Lyn and GSK3, 2 kinases with a predicted impact on the erythroid cytoskeleton, and thus identified an effect of those kinases on the cell's capacity to undergo successive deformations.

Together with Syk, the tyrosine kinase Lyn has been reported to phosphorylate the erythrocyte membrane protein band 3,[33] leading to changes in red cell properties, including membrane stability and intracellular pH.[44] Altered Lyn kinase activity resulting in band 3 hyperphosphorylation and disruption in erythrocyte membrane-cytoskeletal connectivity and compromised RBC stability is among the defining features of the disease chorea-acanthocytosis.[45] The regulation of Lyn activity occurs partially through autophosphorylation of the tyrosine residue in site Y397, which we have detected in this dataset and is well-described to induce further activation of the protein.[34] Interestingly, no phosphorylated tyrosine residues of band 3 were found to be exclusive to mid- or postdeformation samples, although the residue targeted by Lyn kinase (tyrosine 359)

Table 1. Integrative list of deformation-induced phosphorylations in the reticulocyte

Accession no.	Gene symbol	Protein name	Sequence	Count	Site
E9PIJ1	AMPD2	AMP deaminase 2	TDSDSDLQLYK	7*	S190/S197
A0A0U1RQT1	ACAP2	Arf-GAP with coiled-coil, ANK repeat, and PH domain-containing protein 2	SSPSTGSLDSGNESK	7*	S384
B7Z3I9	ALAD	Δ-aminolevulinic acid dehydratase	SSPAFGDR	7	S215
P49840	GSK3A	Glycogen synthase kinase-3 α	GEPNVSYICSR	7*	Y279
P49840	GSK3A	Glycogen synthase kinase-3 α	TSSFAEPGGGGGGGGGGPGGSASGPGGTGGGK	7*	S21/S39
E9PK89	RAB3IL1	Guanine nucleotide exchange factor for Rab-3A	TLVITSTPASPNR	7	S168
B4DMA2	HSP90AB1	Heat shock protein HSP 90-β	IEDVGSDEEDDSGKDK	7*	S255
Q9H1E3	NUCKS1	Nuclear ubiquitous casein and cyclin-dependent kinase substrate 1	VVDYSQFQESDDADEDYGR	7*	S19
S4R2Y4	CBX3	Chromobox protein homolog 3	SLSDSESDDSK	6	S93
Q08495	DMTN	Dematin	DSSVPGSPSSIVAK	6	S26
Q9UG54	MAP3K7	Mitogen-activated protein kinase kinase kinase 7	SIQDLTVTGTEPGQVSSR	6	S439
P61006	RAB8A	Ras-related protein Rab-8A	KLEGNSPQGSNQGVK	6	S181/S185
B3KVN0	SLC2A1	Solute carrier family 2, facilitated glucose transporter member 1	TPEELFHPLGADSQV	6	S490
A0A087WYB4	STOML2	Stomatin-like protein 2, mitochondrial	APVPGTPDSLSSGSSR	6	T327
Q8IV54	TSC22D4	TSC22D4 protein	NGSPPPGAPSSR	6	S62
P16157	ANK1	Ankyrin-1	NGASPNEVSSDGTTPLAIAK	5	S759
A0A0U1RQT1	ACAP2	Arf-GAP with coiled-coil, ANK repeat, and PH domain-containing protein 2	YSISLSPPEQQK	5	S521
P27824	CANX	Calnexin	QKSDAEEDGGTVSQEEEDR	5	S564
G3V238	EEF1AKMT2	EEF1A lysine methyltransferase 2	SDKGSPGEDGFVPSALGTR	5	S21
P05198	EIF2S1	Eukaryotic translation initiation factor 2 subunit 1	VVTDTDETELAR	5	T279
F8WAE5	EIF2A	Eukaryotic translation initiation factor 2A	SDKSPDLAPTPAPQSTPR	5	S506
C9JII4	GCFC2	GC-rich sequence DNA-binding factor 2	ELPVPGSAEEEPPSGGGR	5	S40
Q2VPJ6	HSP90AA1	HSP90AA1 protein	DKEVSDDEAEEK	5	S231
D3DWY2	IKBKG	Inhibitor of κ light polypeptide gene enhancer in B-cells, kinase γ	SPPEEPPDFCCPK	5	S387
O60307	MAST3	Microtubule-associated serine/threonine-protein kinase 3	SSENVLDEEGGR	5	S134
F2Z2K0	NSFL1C	NSFL1 cofactor p47	SPNELVDDLFK	5	S114
B7Z8Y1	NFATC2	Nuclear factor of activated T-cells, cytoplasmic 2	TSPDPSPVSAAPSK	5	S330
H0Y5Q9	INPP5D	Phosphatidylinositol 3,4,5-trisphosphate 5-phosphatase 1	GESPPTPPGQPPISPK	5	T963
D6RC77	PGM3	Phosphoacetylglucosamine mutase	STIGVMVTASHNPEEDNGVK	5	S64
M4QHP2	PIEZO1	Piezo-type mechanosensitive ion channel component	SGSEEAVTDPGER	5	S1621
Q9BVG4	PBDC1	Protein PBDC1	GADSGEEKEEGINR	5	S197
B4E3V2	SQSTM1	Sequestosome-1	LTPVSPESSSTEEK	5	T269/S272
Q6PJD5	SHARPIN	SHARPIN protein	SPGNLTER	5	S165
B2RMN7	SPTB	Spectrin β chain	TSPVSLWSR	5	S2114/S2117
C9JWF0	SMC4	Structural maintenance of chromosomes protein 4	REEGPPPPSPDGASSDAEPEPPSGR	5	S22
H0YN01	TLN2	Talin-2	LDEGTPPEPK	5	T1843
C9J3F6	TBC1D5	TBC1 domain family member 5	NISSSPSVESLPGGR	5	S541/S544
E9PJJ0	TBCEL	Tubulin-specific chaperone cofactor E-like protein	YSPENFPYR	5	S18
Q8IXQ3	C9orf40	Uncharacterized protein C9orf40	RDSGDNSAPSGQER	5	S76
Q5JSH3	WDR44	WD repeat-containing protein 44	VGNESPVQELK	5	S50
F8WBS8	PSMD2	26S proteasome non-ATPase regulatory subunit 2	DKAPVQPQQSPAAAPGGTDEKPSGK	4	S16
Q92625	ANKS1A	Ankyrin repeat and SAM domain-containing protein 1A	SESLSNCSIGK	4	S647

List of significantly enriched or exclusive phosphopeptides in reticulocytes after deformation, as assayed through microsphiltration and microcapillary traversal. Generally, only phosphopeptides present in at least 4 of the 7 postdeformation samples (4 microsphiltration + 3 microfluidics) and not present in at least 4 of the 7 predeformation samples were included. The exception to this analysis consists of the phosphopeptides counted as 7*, which were present in all postdeformation samples but also in 4 of 7 of the predeformation samples. The prediction of the most probable phosphosites in the phosphopeptide was included according to the count of occurrences in previous low-throughput and high-throughput studies, as assayed through PhosphoSitePlus.[50]

Table 1. (continued)

Accession no.	Gene symbol	Protein name	Sequence	Count	Site
E9PJP4	EPB41L2	Band 4.1-like protein 2	EVAENQQNQSSDPEEEKGSQPPPAAESQSSLR	4	S39/S58
A8MZ77	BSG	Basigin	RKPEDVLDDDDAGSAPLK	4	S362
Q9NSY1	BMP2K	BMP-2-inducible protein kinase	DSQSSNEFLTISDSK	4	S1029
A0A0C4DGD1	CAST	Calpastatin	DTSQSDKDLDDALDK	4	S563
Q9Y5K6	CD2AP	CD2-associated protein	KNSLDELR	4	S582
Q8TEH3	DENND1A	DENN domain-containing protein 1A	TGGTLSDPEVQR	4	T24
B4DU91	EPN1	Epsin-1	SPGAFDMSGVR	4	S435
M0QXW7	KHSRP	Far upstream element-binding protein 2	VQISPDSGGLPER	4	S181
F5H1C6	FERMT3	Fermitin family homolog 3	TASGDYIDSSWELR	4	Y11
P04075	ALDOA	Fructose-bisphosphate aldolase A	GILAADESTGSIAKR	4	S36
H0YJ30	GPHN	Gephyrin	ASHSAVDITK	4	S303/S305
Q2Q9B7	G6PD	Glucose-6-phosphate 1-dehydrogenase	VQPNEAVYTK	4	Y401
E9PK89	RAB3IL1	Guanine nucleotide exchange factor for Rab-3A	ELHPQLLSPTK	4	S179
O75633	GNAS	Guanine nucleotide-binding protein Gs α subunit isoform L3	ISTASGDGR	4	S352
Q5H924	HUWE1	HECT, UBA, and WWE domain containing 1	REESPMDVDQPSPSAQDTQSIASDGTPQGEK	4	S3816
A0A0F7NGI8	LRRFIP1	Leucine rich repeat	IDGATQSSPAEPK	4	S714
E9PJF4	CLNS1A	Methylosome subunit pICln	EPVADEEEEDSDDDVEPITEFR	4	S102
S4R3D6	APIP	Methylthioribulose-1-phosphate dehydratase	DISGPSPSKK	4	S87
Q6NT16	SLC18B1	MFS-type transporter SLC18B1	SKSQNILSTEEER	4	S438
B4DS42	OATL1	Ornithine aminotransferase-like 1	QASLDGLQQLR	4	S506
P30041	PRDX6	Peroxiredoxin-6	DFTPVCTTELGR	4	T44
I3L1U0	RILP	Rab-interacting lysosomal protein	AESSEDETSSPAPSK	4	S354
Q9P227	ARHGAP23	ρ GTPase-activating protein 23	SAEALGPGALVSPR	4	S361/S372
Q16513	PKN2	Serine/threonine-protein kinase N2	ASSLGEIDESSELR	4	S583
C9JIG9	OXSR1	Serine/threonine-protein kinase OSR1	TEDGGWEWSDDEFDEESEEGK	4	S339
P02549	SPTA1	Spectrin α chain, erythrocytic 1	QDTLDASLQSFQQER	4	S1976
B2RMN7	SPTB	Spectrin β chain	LSSSWESLQPEPSHPY	4	S2123/S2125/S2128
B4DZC9	SLK	STE20-like serine/threonine-protein kinase	VDEDSAEDTQSNDGK	4	S571
P17987	TCP1	T-complex protein 1 subunit α	HGSYEDAVHSGALND	4	S544/Y545
B4DUI5	TPI1	Triosephosphate isomerase	IIYGGSVTGATCK	4	Y246
Q8IV54	TSC22D4	TSC22D4 protein	VEAEAGGSGARTPPLSR	4	T229
B4DQ79	LYN	Tyrosine-protein kinase	VIEDNEYTAR	4	Y397
A0A024R8I2	UBADC1	Ubiquitin associated domain containing 1, isoform CRA_c	APSPLPK	4	S98
Q5VVQ6	YOD1	Ubiquitin thioesterase OTU1	SSPAFTK	4	S130
B3KW31	VPS13A	Vacuolar protein sorting 13A	QASFTDVRDPSLK	4	S1416
A0A0S2Z3K9	CRK	V-crk sarcoma virus CT10 oncogene-like protein isoform 2	DSSTSPGDYVLSVSENSR	4	S41

List of significantly enriched or exclusive phosphopeptides in reticulocytes after deformation, as assayed through microsphiltration and microcapillary traversal. Generally, only phosphopeptides present in at least 4 of the 7 postdeformation samples (4 microsphiltration + 3 microfluidics) and not present in at least 4 of the 7 predeformation samples were included. The exception to this analysis consists of the phosphopeptides counted as 7*, which were present in all postdeformation samples but also in 4 of 7 of the predeformation samples. The prediction of the most probable phosphosites in the phosphopeptide was included according to the count of occurrences in previous low-throughput and high-throughput studies, as assayed through PhosphoSitePlus.[50]

was observed to be phosphorylated across all samples. It is important to note that our experimental analysis is focused on the identification of phosphopeptides which are uniquely associated with deformation. Therefore, basally phosphorylated proteins for which deformation-induced changes constitute an alteration in abundance of the phosphorylated population would not be included in our list. This approach will undoubtedly result in a smaller list of candidate deformation-associated modifications relative to that which could be achieved using comparative quantitative alternatives (such as TMT labeling). Nevertheless, it both enables a greater input of material to be used (increasing the likelihood of detecting phosphopeptides that are only present in low abundance) and, crucially, generates targets that are easier to modulate experimentally because no quantity-based effects need to be accounted for

when interfering with protein activity (given that these modifications are not present in the nondeformed cell and thus are not essential for their survival, at least in vitro).

In contrast to Lyn, the impact of GSK3α in RBCs is markedly less well-characterized. GSK3 is a serine/threonine kinase which has been shown to phosphorylate multiple sites in β-adducin and consequently regulate its activity in cortical neurons.[35] In erythrocytes, β-adducin interacts with band 3 and with the spectrin-actin cytoskeleton, stabilizing the junctional complex and regulating membrane deformability.[36] No phosphorylated residue of β-adducin was detected in our datasets to be exclusive to cells undergoing or recovering from deformation; however, given the presence of the GSK3-phosphorylated β-adducin peptide in the predeformation samples and the previously described limitations, it is tantalizing to speculate that modification of this site could be involved in the regulation of membrane-cytoskeletal connectivity of RBCs.

Interestingly, a compounding effect was repeatedly observed when inhibiting the 2 kinases, suggesting the existence of independent mechanisms that are activated by the same initial stimulus. However, neither inhibitor affected the inherent capacity of the cells to undergo deformation (as assessed by rheoscopy) in contrast to treatment with an anti-GPA antibody. Although we cannot exclude that varying shear stress levels or exposure times induced by the different modalities may contribute to this result, we hypothesize that inhibiting these mechanisms results in an inability to recover from successive deformations rather than an inability to deform. The initial deformability of the cell could, therefore, be primarily related to its inherent biophysical properties[46] and not necessarily to a signaling pathway response (especially given the very short timeframe required for deformation). Nonetheless, as showcased by our functional assay studies, kinase activity and thus phosphorylation is clearly an important event in the regulation of physiological deformation.

In conclusion, our results not only present previously undescribed mechanisms for shear stress and deformation response in human erythrocytes and reticulocytes, but also serve as a valuable resource for further mechanistic dissection of the molecular pathways that underlie the RBC's response to mechanical stimuli and for the study of reticulocyte maturation.

Acknowledgments

The authors thank Stephanie Pellegrin (University of Bristol, Bristol, United Kingdom) for her contributions to $CD34^+$ cell isolation and culture; Kate Heesom and Marieangela Wilson, as well as the proteomics facility of the University of Bristol, for proteomics sample processing and data acquisition; Stephen Cross, as well as the Wolfson Bioimaging Facility of the University of Bristol, for helpful discussions and macro creation for imaging data preprocessing; and Judith Cluitmans (Radboud University Medical Center, Nijmegen, The Netherlands) for support in initial establishment of microsphiltration assays.

P.L.M. was funded by the European Union (H2020-MSCA-ITN-2015, "RELEVANCE," grant agreement number 675117). M.A.L.I. and W.E.N. were funded by the INSERM, the Institut National de la Transfusion Sanguine, and the Laboratory of Excellence GR-Ex, reference ANR-11-LABX-0051; GR-Ex is funded by the program "Investissements d'avenir" of the French National Research Agency, reference ANR-11-IDEX-0005-02. M.A.L.I. was additionally funded by the Ministère de l'Enseignement Supérieur et de la Recherche (Ecole Doctorale BioSPC) and received financial support from the Club du Globule Rouge et du Fer and the Société Française d'Hématologie. O.F. and B.L.P. acknowledge the Labex LaSIPS (ANR-10-LABX-0040-Lasips), the Institut d'Alembert and the CNRS for project funding (microfluidics). A.M.T. and T.J.S. were funded by a National Health Service Blood and Transplant research and development grant (WP15-04 and WP15-05) and the National Institute for Health Research Blood and Transfusion Research Unit (NIHR BTRU) in Red Cell Products (NIHR-BTRU-2015-10032).

The views expressed are those of the authors and not necessarily those of the National Health Service, NIHR, or the Department of Health and Social Care.

Authorship

Contribution: P.L.M. performed the majority of experiments, analyzed data, and prepared figures; M.A.L.I. and P.L.M. performed microfluidics experiments under supervision of W.E.N.; O.F. and B.L.P. provided essential reagents for microfluidics experiments; J.G.G.D. and G.J.S. provided essential Automated Rheoscope and Cell Analyzer equipment and analysis software; P.L.M, M.A.L.I., W.E.N., A.M.T., and T.J.S. conceived and designed experiments; P.L.M., A.M.T., and T.J.S. wrote the manuscript; A.M.T. and T.J.S. contributed equally to conception and supervision of the work; and all authors read and edited the manuscript.

Conflict-of-interest disclosure: The authors declare no competing financial interests.

ORCID profiles: P.L.M., 0000-0002-0493-5394; W.E.N., 0000-0001-8184-427X; A.M.T., 0000-0003-4395-9396; T.J.S., 0000-0003-0590-292X.

Correspondence: Timothy J. Satchwell, School of Biochemistry, University of Bristol, Medical Science Building, University Walk, Bristol BS8 1TD, United Kingdom; e-mail: t.satchwell@bristol.ac.uk; or Ashley M. Toye, School of Biochemistry, University of Bristol, Medical Science Building, University Walk, Bristol BS8 1TD, United Kingdom; e-mail: ash.m.toye@bristol.ac.uk.

References

1. Malleret B, Xu F, Mohandas N, et al. Significant biochemical, biophysical and metabolic diversity in circulating human cord blood reticulocytes. *PLoS One*. 2013;8(10):e76062.
2. Xie L, Sun D, Yao W, Wen Z. Microrheological characteristics of reticulocyte in vivo. *Sci China C Life Sci*. 2002;45(1):50-56.
3. Malleret B, Li A, Zhang R, et al. Plasmodium vivax: restricted tropism and rapid remodeling of CD71-positive reticulocytes. *Blood*. 2015;125(8):1314-1324.
4. Wan J, Ristenpart WD, Stone HA. Dynamics of shear-induced ATP release from red blood cells. *Proc Natl Acad Sci USA*. 2008;105(43):16432-16437.

5. Cinar E, Zhou S, DeCourcey J, Wang Y, Waugh RE, Wan J. Piezo1 regulates mechanotransductive release of ATP from human RBCs. *Proc Natl Acad Sci USA*. 2015;112(38):11783-11788.
6. Holroyde CP, Gardner FH. Acquisition of autophagic vacuoles by human erythrocytes. Physiological role of the spleen. *Blood*. 1970;36(5):566-575.
7. King JS, Veltman DM, Insall RH. The induction of autophagy by mechanical stress. *Autophagy*. 2011;7(12):1490-1499.
8. Cahalan SM, Lukacs V, Ranade SS, Chien S, Bandell M, Patapoutian A. Piezo1 links mechanical forces to red blood cell volume. *eLife*. 2015;4:4.
9. Faucherre A, Kissa K, Nargeot J, Mangoni ME, Jopling C. Piezo1 plays a role in erythrocyte volume homeostasis. *Haematologica*. 2014;99(1):70-75.
10. Zipser Y, Piade A, Barbul A, Korenstein R, Kosower NS. Ca2+ promotes erythrocyte band 3 tyrosine phosphorylation via dissociation of phosphotyrosine phosphatase from band 3. *Biochem J*. 2002;368(Pt 1):137-144.
11. Coussens L, Parker PJ, Rhee L, et al. Multiple, distinct forms of bovine and human protein kinase C suggest diversity in cellular signaling pathways. *Science*. 1986;233(4766):859-866.
12. Govekar RB, Zingde SM. Protein kinase C isoforms in human erythrocytes. *Ann Hematol*. 2001;80(9):531-534.
13. Kostova EB, Beuger BM, Klei TR, et al. Identification of signalling cascades involved in red blood cell shrinkage and vesiculation. *Biosci Rep*. 2015;35(2): e00187.
14. Patel VP, Fairbanks G. Spectrin phosphorylation and shape change of human erythrocyte ghosts. *J Cell Biol*. 1981;88(2):430-440.
15. Pinder JC, Bray D, Gratzer WB. Control of interaction of spectrin and actin by phosphorylation. *Nature*. 1977;270(5639):752-754.
16. Boivin P. Role of the phosphorylation of red blood cell membrane proteins. *Biochem J*. 1988;256(3):689-695.
17. Lavazec C, Deplaine G, Safeukui I, et al. Microsphiltration: a microsphere matrix to explore erythrocyte deformability. *Methods Mol Biol*. 2013;923: 291-297.
18. Waugh RE. Reticulocyte rigidity and passage through endothelial-like pores. *Blood*. 1991;78(11):3037-3042.
19. Lizarralde Iragorri MA, El Hoss S, Brousse V, et al. A microfluidic approach to study the effect of mechanical stress on erythrocytes in sickle cell disease. *Lab Chip*. 2018;18(19):2975-2984.
20. Duez J, Carucci M, Garcia-Barbazan I, et al. High-throughput microsphiltration to assess red blood cell deformability and screen for malaria transmission-blocking drugs. *Nat Protoc*. 2018;13(6):1362-1376.
21. Griffiths RE, Kupzig S, Cogan N, et al. Maturing reticulocytes internalize plasma membrane in glycophorin A-containing vesicles that fuse with autophagosomes before exocytosis. *Blood*. 2012;119(26):6296-6306.
22. Dobbe JG, Streekstra GJ, Hardeman MR, Ince C, Grimbergen CA. Measurement of the distribution of red blood cell deformability using an automated rheoscope. *Cytometry*. 2002;50(6):313-325.
23. Moura PL, Hawley BR, Mankelow TJ, et al. Non-muscle myosin II drives vesicle loss during human reticulocyte maturation. *Haematologica*. 2018;103(12): 1997-2007.
24. Deplaine G, Safeukui I, Jeddi F, et al. The sensing of poorly deformable red blood cells by the human spleen can be mimicked in vitro. *Blood*. 2011;117(8): e88-e95.
25. Schindelin J, Arganda-Carreras I, Frise E, et al. Fiji: an open-source platform for biological-image analysis. *Nat Methods*. 2012;9(7):676-682.
26. Betz T, Lenz M, Joanny JF, Sykes C. ATP-dependent mechanics of red blood cells. *Proc Natl Acad Sci USA*. 2009;106(36):15320-15325.
27. Huisjes R, Bogdanova A, van Solinge WW, Schiffelers RM, Kaestner L, van Wijk R. Squeezing for Life - Properties of Red Blood Cell Deformability. *Front Physiol*. 2018;9:656.
28. Azouzi S, Romana M, Arashiki N, et al. Band 3 phosphorylation induces irreversible alterations of stored red blood cells. *Am J Hematol*. 2018;93(5): E110-E112.
29. Fairbanks G, Palek J, Dino JE, Liu PA. Protein kinases and membrane protein phosphorylation in normal and abnormal human erythrocytes: variation related to mean cell age. *Blood*. 1983;61(5):850-857.
30. Mankelow TJ, Griffiths RE, Trompeter S, et al. The ins and outs of reticulocyte maturation revisited: the role of autophagy in sickle cell disease. *Autophagy*. 2016;12(3):590-591.
31. Huang da W, Sherman BT, Lempicki RA. Systematic and integrative analysis of large gene lists using DAVID bioinformatics resources. *Nat Protoc*. 2009; 4(1):44-57.
32. Huang da W, Sherman BT, Lempicki RA. Bioinformatics enrichment tools: paths toward the comprehensive functional analysis of large gene lists. *Nucleic Acids Res*. 2009;37(1):1-13.
33. Brunati AM, Bordin L, Clari G, et al. Sequential phosphorylation of protein band 3 by Syk and Lyn tyrosine kinases in intact human erythrocytes: identification of primary and secondary phosphorylation sites. *Blood*. 2000;96(4):1550-1557.
34. Katagiri T, Ogimoto M, Hasegawa K, et al. CD45 negatively regulates lyn activity by dephosphorylating both positive and negative regulatory tyrosine residues in immature B cells. *J Immunol*. 1999;163(3):1321-1326.
35. Farghaian H, Turnley AM, Sutherland C, Cole AR. Bioinformatic prediction and confirmation of beta-adducin as a novel substrate of glycogen synthase kinase 3. *J Biol Chem*. 2011;286(28):25274-25283.
36. Franco T, Low PS. Erythrocyte adducin: a structural regulator of the red blood cell membrane. *Transfus Clin Biol*. 2010;17(3):87-94.
37. Goc A, Al-Husein B, Katsanevas K, et al. Targeting Src-mediated Tyr216 phosphorylation and activation of GSK-3 in prostate cancer cells inhibit prostate cancer progression in vitro and in vivo. *Oncotarget*. 2014;5(3):775-787.

38. Chasis JA, Reid ME, Jensen RH, Mohandas N. Signal transduction by glycophorin A: role of extracellular and cytoplasmic domains in a modulatable process. *J Cell Biol*. 1988;107(4):1351-1357.

39. Cluitmans JC, Gevi F, Siciliano A, et al. Red blood cell homeostasis: pharmacological interventions to explore biochemical, morphological and mechanical properties. *Front Mol Biosci*. 2016;3:10.

40. Wilson MC, Trakarnsanga K, Heesom KJ, et al. Comparison of the proteome of adult and cord erythroid cells, and changes in the proteome following reticulocyte maturation. *Mol Cell Proteomics*. 2016;15(6):1938-1946.

41. Chu TTT, Sinha A, Malleret B, et al. Quantitative mass spectrometry of human reticulocytes reveal proteome-wide modifications during maturation. *Br J Haematol*. 2018;180(1):118-133.

42. Prenni JE, Vidal M, Olver CS. Preliminary characterization of the murine membrane reticulocyte proteome. *Blood Cells Mol Dis*. 2012;49(2):74-82.

43. Gautier EF, Leduc M, Cochet S, et al. Absolute proteome quantification of highly purified populations of circulating reticulocytes and mature erythrocytes. *Blood Adv*. 2018;2(20):2646-2657.

44. Puchulu-Campanella E, Turrini FM, Li YH, Low PS. Global transformation of erythrocyte properties via engagement of an SH2-like sequence in band 3. *Proc Natl Acad Sci USA*. 2016;113(48):13732-13737.

45. De Franceschi L, Tomelleri C, Matte A, et al. Erythrocyte membrane changes of chorea-acanthocytosis are the result of altered Lyn kinase activity. *Blood*. 2011;118(20):5652-5663.

46. Pivkin IV, Peng Z, Karniadakis GE, Buffet PA, Dao M, Suresh S. Biomechanics of red blood cells in human spleen and consequences for physiology and disease [published correction appears in *Proc Natl Acad Sci USA*. 2017;114(22):E4521]. *Proc Natl Acad Sci USA*. 2016;113(28):7804-7809.

47. Vizcaíno JA, Csordas A, del-Toro N, et al. 2016 update of the PRIDE database and its related tools. *Nucleic Acids Res*. 2016;44(D1):D447-D456.

48. Duez J, Holleran JP, Ndour PA, et al. Splenic retention of Plasmodium falciparum gametocytes to block the transmission of malaria. *Antimicrob Agents Chemother*. 2015;59(7):4206-4214.

49. Jensen LJ, Kuhn M, Stark M, et al. STRING 8--a global view on proteins and their functional interactions in 630 organisms. *Nucleic Acids Res*. 2009;37(database issue):D412-D416.

50. Hornbeck PV, Zhang B, Murray B, Kornhauser JM, Latham V, Skrzypek E. PhosphoSitePlus, 2014: mutations, PTMs and recalibrations. *Nucleic Acids Res*. 2015;43(database issue):D512-D520.

51. Tinevez JY, Perry N, Schindelin J, et al. TrackMate: an open and extensible platform for single-particle tracking. *Methods*. 2017;115:80-90.